
Error Diffusion: Post Training Quantization with Block-Scaled Number Formats for Neural Networks

Alireza Khodamoradi*

Kristof Denolf

Eric Dellinger

first.last@amd.com

Abstract

Quantization reduces the model’s hardware costs, such as data movement, storage, and operations like multiply and addition. It also affects the model’s behavior by degrading the output quality. Therefore, there is a need for methods that preserve the model’s behavior when quantizing model parameters. More exotic numerical encodings, such as block-scaled number formats, have shown advantages for utilizing a fixed bit budget to encode model parameters. This paper presents error diffusion (ED), a hyperparameter-free method for post-training quantization with support for block-scaled data formats. Our approach does not rely on backpropagation or Hessian information. We describe how to improve the quantization process by viewing the neural model as a composite function and diffusing the quantization error in every layer. In addition, we introduce TensorCast, an open-source library based on PyTorch to emulate a variety of number formats, including the block-scaled ones, to aid the research in neural model quantization. We demonstrate the efficacy of our algorithm through rigorous testing on various architectures, including vision and large language models (LLMs), where it consistently delivers competitive results. Our experiments confirm that block-scaled data formats provide a robust choice for post-training quantization and could be used effectively to enhance the practical deployment of advanced neural networks.

1 Introduction

The rise in popularity of neural models as an instrumental technology for integrating intelligence into electronic devices has increased the demand for innovative and efficient implementations of these models. They are constantly growing in size (number of parameters) and complexity (layer connections and their functions) [1]. More parameters require more operations (e.g., multiply and addition) [2, 3], more memory for storage [4], and larger bandwidth for data movement [5]. Complex connections [6, 7] and complex functions (e.g., SoftMax) require caching, data movement orchestration, and more computation [8, 9].

Quantizing model parameters enables the use of denser, faster, and cheaper operations [10], and reduces memory, caching, and data movement requirements [11, 2]. These substantial reductions in hardware costs are excellent incentives to quantize neural models and rigorously address and mitigate quantization’s negative effect on the model behavior and performance [12–14].

The negative quantization effect on neural models is also known as the quantization error, and it increases when smaller number formats are used for quantization. Converting from 32-bit number formats (fp32) to 16-bit number formats (e.g., fp16 and bfloat16) can be done through simple casting while quantizing to 8-bit number formats (e.g., fp8 and int8) is a more sensitive process and may

*Corresponding Author.

require per-channel, per-tensor, or per-kernel scales [15–18]. Quantizing to sub-8-bit number formats (e.g., int4) is more challenging and requires sophisticated methods [19, 20], mainly due to limited precision and dynamic range of these number formats [21, 22].

Block-scaled numerical formats [23, 24] have recently gained popularity in AI applications due to their numerical advantages, such as increased dynamic range over non-scaled data formats [25–27].

Current post-training quantization methods are not designed with block-scaled number formats in mind and do not capture their specific characters, such as the dependency created by the shared scale between the values in a block. They also focus only on the layers being quantized, and their algorithms do not process layers that are not quantized.

The ED method is the first PTQ algorithm supporting power-of-two block-scaled number formats and is designed to respect the data layout of these number formats. Because a block-scaled number format with a block size of one is technically a non-block-scaled number format, the ED algorithm also works and supports non-block-scaled number formats. In addition, this work introduces TensorCast, a PyTorch-based library to emulate a variety of data formats to assist researchers and engineers in their experiments in neural model quantization. We provide examples of how to use the TensorCast and quantize neural models with block-scaled data formats. Our innovations in the Error Diffusion PTQ method can be summarized as:

- A novel weighted adjust-and-quantize method.
- Specialized support for block-scaled number formats.
- Introducing TensorCast, an open-source PyTorch library to support block-scaled data formats for quantization

The rest of this article is organized as follows: section 2 reviews neural model quantization and related work. Section 3 covers the details of the block-scaled data formats. Section 4 describes Error Diffusion in detail. Section 5 introduces TensorCast library. Section 6 discusses our results, and section 7 provides further discussion and our conclusions.

2 Neural Model Quantization

The neural network model is a set of layers, and its architecture connections are described with a directed acyclic graph (DAG). The model layers are the edges of this DAG, and they are functions mapping activation tensors (the nodes in the DAG) to activation tensors.

For example, model Φ in Figure 1, is composed of four layers. The input to Φ , x is the input to $f^{(1)}$ and its output, $f^{(1)}(x)$ is input to $f^{(2)}$ which maps it to $f^{(2)}(f^{(1)}(x))$. $f^{(3)}$ takes two inputs, one is the output of $f^{(1)}$ and the other one is the output of $f^{(2)}$ and can be shown as $f^{(3)}(f^{(2)}(f^{(1)}(x)), f^{(1)}(x))$. In this text, we adopt a more simple form by using the symbol \circ and rewrite this relation as $f^{(3)} \circ (f^{(2)} \circ f^{(1)}, f^{(1)})$. Therefore, the model composite function composed of these four layer functions is shown as $\Phi = f^{(4)} \circ f^{(3)} \circ (f^{(2)} \circ f^{(1)}, f^{(1)})$.

Let’s assume $f^{(2)}$ is the affine map of a linear layer $f^{(2)}(A) = AW^T + b$. Quantizing the weight matrix W to \widehat{W} , changes this map to $\widehat{f}^{(2)}(A) = A\widehat{W}^T + b$ and, consequently, changes the model function to $\widehat{\Phi} = f^{(4)} \circ f^{(3)} \circ (\widehat{f}^{(2)} \circ f^{(1)}, f^{(1)})$.

One way to correct this change is to compile the new model function, $\widehat{\Phi}$, to behave similar to Φ . The training process of a neural network is the compilation process of the model function. Applying quantization during the model training stage and correcting for its effect on the model function is known as quantization-aware training (QAT) [28–32].

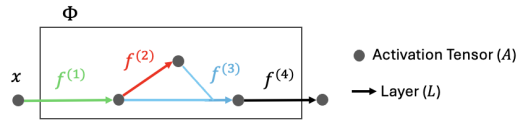


Figure 1: Model $\Phi = f^{(4)} \circ f^{(3)} \circ (f^{(2)} \circ f^{(1)}, f^{(1)})$ as a composite function with dependencies described by its DAG. Each function’s connections is color-coded to show its inputs and output.

In the QAT process, the effect of the quantization on the model’s output is captured by a loss function. The backpropagation can then suggest changing any model parameter to optimize for the loss function. Therefore, any combination of parameters in the whole model could be changed to correct the quantization effect. This process provides much flexibility and potential for compiling a quantized model with high performance. However, the training process requires vast computational resources [33], human expertise to adjust the training script [34, 35], and access to the training dataset that could be restricted by proprietary restrictions.

Another way to quantize a model is to apply the quantization after the training stage. This is also known as post-training quantization (PTQ). The PTQ process is computationally simpler than the QAT and does not require the training dataset. Given the high cost of training large language models [34, 36], PTQ is a cost-efficient option for quantizing and calibrating a neural model for a specific task(s).

However, quantizing trained parameters significantly and adversely changes the model’s behavior. Therefore, it is preferred for the PTQ methods to include methods to correct this change and reduce the quantization error. Popular PTQ algorithms measure the quantization changes in the model and suggest better rounding or update terms for model parameters [21, 20, 19]. In this text, we refer to this process in PTQ, as model calibration.

The calibration of the model function in PTQ can be divided into multiple more straightforward tasks of calibrating its subfunctions. This is referred to as layer-wise calibration. Early works ([37, 38]) proposed the calibration in PTQ as minimizing the distance between the weights of each layer, $W^{(l)}$, and their quantized version, $\widehat{W}^{(l)}$, as:

$$\widehat{W}^{(l)} = \arg \min_{\widehat{W}^{(l)}} \|W^{(l)} - \widehat{W}^{(l)}\|_2^2 \quad (1)$$

Other works, such as [39, 31], proposed improving Equation 1 by measuring the changes at the layer’s output instead of its parameters. Taking Φ in Figure 1 as an example, quantization converts the weights, W , of each function, f , from a higher-precision number format to \widehat{W} represented in simpler, lower-precision number format. Therefore, the output of layer function l changes from $f^{(l)}(A, W^{(l)})$ to $f^{(l)}(\widehat{A}, \widehat{W}^{(l)})$. Here, \widehat{A} denote the quantization effect of every layer before layer l in the model DAG on this layer’s input. A distance function \mathcal{D} can measure the difference in each layer output to indicate functional change caused by the quantization. In this case, the calibration process in PTQ aims to minimize this distance instead of the one shown in Equation 1.

A popular choice for \mathcal{D} is the l_2 -norm [40, 20, 19]. Hence, the calibration goal is to find $\widehat{W}^{(l)}$ as:

$$\arg \min_{\widehat{W}} \|AW^T - \widehat{A}\widehat{W}^T\|_2^2 \quad (2)$$

The OBS framework [41, 42] assumes $\widehat{A} = A$ and suggests quantizing each weight using the inverse Hessian information and updating the remaining non-quantized weights for PTQ calibration. However, in its proper form, this approach is computationally very demanding at $O(n^4)$ total runtime, with n being the number of model parameters. To overcome this complexity, [40] sets $\widehat{A} = A$ in Equation 2 and changes the l_2 -norm term to $\sum_i \|AW_{i,:}^T - A\widehat{W}_{i,:}^T\|_2^2$. This way, all the W rows have standard least squares form, and the Hessian calculation will be reduced to $H = 2XX^T$. Later, GPTQ [20], optimized this Hessian calculation by using the same order for all the rows and improving its numerical stability using Cholesky reformulation.

In this work, we also use the l_2 -norm to measure the changes in each output. Our method is based on GPFQ [19] and propagates the quantization effect through the model DAG ($\widehat{A} \neq A$ in Equation 2). This means that if $f^{(1)}$ in Figure 1 is quantized and replaced by $\widehat{f}^{(1)}$, the input to $\widehat{f}^{(2)}$ will be different than the input to $f^{(2)}$, and our algorithm tries to minimize the difference between $f^{(2)}$ and $\widehat{f}^{(2)}$ outputs when their inputs are different.

In addition, our PTQ method also calibrates layers that are not being quantized and supports block-scaled data formats and their data layout (more detail in Section 4). Before explaining the ED algorithm, we briefly review the block-scaled data formats in the next section.

3 Block-scaled number formats

A number format represents a range of numerical values within a budget of space measured in bits. It is a design choice that balances the number encoding capacity with energy and area. The resolution separating two close values is the number format’s precision, and its dynamic range indicates how far-apart values can be encoded by it. High precision and wide dynamic range require large bit budgets. The number of bits used by a number format indicates its alphabet size². However, number formats with larger bit budgets are more expensive to support in hardware. For example, the IEEE 754 fp32 number format can encode positive values from 1.4×10^{-45} to 3.4×10^{38} and has an alphabet size of 2^{32} , while the fp8(e4m3) [43] number format can encode positive values from 1.9×10^{-3} to 448 and has an alphabet size of 2^8 . The storage and data movement for fp32 values requires four times more memory and energy than fp8, and modern computing units can perform 16x more floating operations on fp8 values than fp32 values in the same number of clock cycles [44].

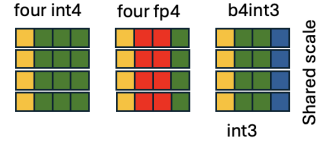


Figure 2: Bit layout for four values encoded in int4 (sign: 1 bit and mantissa: 3 bits), fp4 (sign: 1 bit, exponent: 2 bits, and mantissa: 1 bit), and b4int3 (sign: 1 bit, mantissa: 2 bits, and 4-bit scale).

Previous works [25–27] have shown the benefit of quantizing neural models with block-scaled number formats. These data formats have also gained large support from the computing hardware community [43]. Block-scaled data formats share a few bits between a group of values to scale them together. Proper scaling can help with encoding weights at the quantization time by better matching the weights’ distribution. It also creates a dependency between the values inside each block.

For example, we can encode four values with int4, fp4, or b4int3 (Figure 2). In the block-scaled number format, b4int3, each value has a private int3 data format, and every four values share a 4-bit scale. Int4 and fp4 encode $\pm\{0, 1, 2, 3, 4, 5, 6, 7\}$ and $\pm\{0, 0.5, 1, 1.5, 2, 3, 4, 6\}$, their dynamic ranges³ are 7 and 12, and their precisions are 1 and 0.5, respectively. The alphabet size for int4 and fp4 is 15 ($+0 = -0$). With b4int3, 16 different shared scales can scale the seven int3 values and create 67 unique numbers between $\pm 3 \times 2^8$ and $\pm 2^{-7}$. If each value’s private bits encode a numerical value p_i and shared scale bits encode a numerical value s_b in the block-scaled number format, each value can be calculated as:

$$w_i = s_b \times p_i \quad (3)$$

The shared scale in b4int3 encodes a power of two number. Therefore the above equation is just a shift in hardware and is highly desired for low-power high-performance chips. Note that int4 and fp4 cannot encode anything smaller than ± 0.5 or larger than ± 7 . While b4int3 can scale the int3 values to larger or smaller numbers. However, only four different numbers are available for encoding a block with each scale. Therefore, the quantization errors for all the values inside a block depend on the selected scale. This is the dependency inside a block encoded with block-scaled data format. The following section describes how our PTQ algorithm accounts for this dependency.

4 Error Diffusion (ED)

The output of a linear layer with input activations $A_{M \times IFM}$ and weight matrix $W_{OFM \times IFM}$, is $O_{M \times OFM} = AW^T$ (Figure 3, top left). We re-write this matrix multiply as following:

$$O = \bigcup_{i=1}^M \bigcup_{j=1}^{OFM} \sum_{k=1}^{IFM} o_{i,j}^{(k)} = \sum_{k=1}^{IFM} \bigcup_{i=1}^M \bigcup_{j=1}^{OFM} o_{i,j}^{(k)} = \sum_{k=1}^{IFM} A_{:,k} (W_{:,k})^T = \sum_{k=1}^{IFM} O^{(k)} \quad (4)$$

²alphabet size is the number of different possible encodings (2^b for b bits) that can be used to encode numbers, NaN, infinity, etc.

³in this text we define the dynamic range as largest-in-magnitude value divided by smallest-in-magnitude and non-zero value

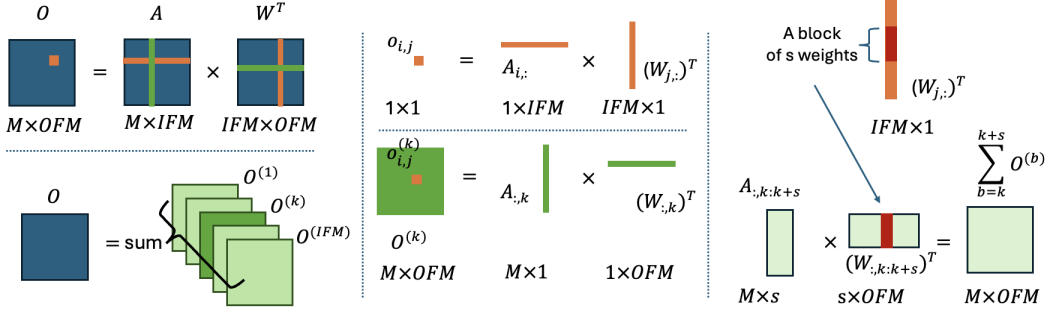


Figure 3: Top left: output, $O_{M \times OFM}$, generated by the matrix multiply of the input activations and weights. Top middle: each element of the output $o_{i,j}$ is the sum of products of two vectors with size $1 \times IFM$. Bottom middle: k th portion of the output matrix is the outer product of two vectors with sizes $M \times 1$ and $1 \times OFM$. Left bottom: output is the sum of its IFM portions. Top Right: a block of s numbers in $(W_{j,:})^T$ column. Bottom right: same block of s numbers expands over s rows $(W_{:,k:k+s})^T$ and effects s output portions.

Here, $o_{i,j} = \sum_{k=1}^{IFM} a_{i,k} * w_{j,k}$ is the output at (i, j) (Figure 3, top middle), and $o_{i,j}^{(k)} = a_{i,k} * w_{j,k}$ is the k th portion of it (Figure 3, the orange square at bottom middle). $O^{(k)} = A_{:,k}(W_{:,k})^T$ (Figure 3, bottom middle) is the k th portion of O (Figure 3, bottom left), and is generated by the k th column of A and W (or k th row of W^T).

Let's denote the quantized weights as \widehat{W} , and use \widehat{A} to denote the activation tensors in the quantized model. For simplicity, we use \widehat{W}_k^T instead of $(\widehat{W}_k)^T$, and k instead of $(:, k)$. Therefore, k th portion of a quantized layer's output is $\widehat{O}^{(k)} = \widehat{A}_k \widehat{W}_k^T$.

We define the quantization error matrix as difference between the original and quantized outputs:

$$E^{(k)} = A_k W_k^T - \widehat{A}_k \widehat{W}_k^T \quad (5)$$

[19] shows that the output of a convolution layer can also be analysed this way.

4.1 Weighted Error Matrix

The greedy path-finding quantization (GPFQ) explained in [19] is only aware of the accumulated error generated by processing the prior iterations (the term $U^{(k-1)}$). We propose to diffuse the quantization error by looking at the whole input matrices A and \widehat{A} at each k th step. Therefore, we start with the following goal:

$$\sum_{k=1}^{IFM} E^{(k)} = (A - \widehat{A})W^T + \sum_{k=1}^{IFM} \widehat{A}_k (W_k^T - \widehat{W}_k^T) = \tilde{O} + \sum_{k=1}^{IFM} \widehat{A}_k (W_k^T - \widehat{W}_k^T) = 0 \quad (6)$$

Here, $\tilde{O} = (A - \widehat{A})W^T$ is the error in layer's input, inherited from prior quantized layers. Ideally, we need scalars $\alpha^{(k)}$ such that $\sum_{k=1}^{IFM} \widehat{A}_k (W_k^T - \widehat{W}_k^T) + \alpha^{(k)} \tilde{O} = 0$. Heuristically, We observed that $\alpha^{(k)} = \frac{1}{IFM}$ is a sufficient term to divide Equation 7 into the iterative following sub-goals:

$$U^{(k)} = \frac{\tilde{O}}{IFM} + \widehat{A}_k (W_k^T - \widehat{W}_k^T) + U^{(k-1)} = 0 \quad (7)$$

Therefore, ED's update and quantization equations are:

$$\widehat{W}_k^T = W_k^T + \frac{\widehat{A}_k^T}{\|\widehat{A}_k\|_2^2} \left(\frac{\tilde{O}}{IFM} + U^{(k-1)} \right) \quad (8)$$

$$\widehat{W}_k^T = \text{quant}\left\{W_k^T + \frac{\widehat{A}_k^T}{\|\widehat{A}_k\|_2^2} \left(\frac{\tilde{O}}{IFM} + U^{(k-1)}\right)\right\} \quad (9)$$

Note that Equation 8 has no hyperparameters and for $A = \widehat{A}$, it describes the same function as [19].

4.2 Calibrating the neural model as a composite function

In many quantization applications, some layers, such as the last layer, are kept unquantized [19, 20]. Similarly, we also update these layers with Equation 8 to better diffuse the error in the model. Take the model in Figure 1, let's assume we quantize layers $f^{(1)}$, $f^{(2)}$, and $f^{(3)}$ to $\widehat{f}^{(1)}$, $\widehat{f}^{(2)}$, and $\widehat{f}^{(3)}$ respectively and keep $f^{(4)}$ unquantized. Hence the quantized model is $\widehat{\Phi} = f^{(4)} \circ \widehat{f}^{(3)} \circ (\widehat{f}^{(2)} \circ \widehat{f}^{(1)}, \widehat{f}^{(1)})$.

Intuitively, all activation tensors are tensor spaces that encode information about the model input and are the same mathematical object. The quantization error flowing in the model through activation functions ($A - \widehat{A}$) are also the same mathematical objects as the activation functions. Layer functions map their input activation tensors to output activation tensors, in fact, they map mathematical objects to the same objects (endofunctions). This means the same mathematical objects are flowing through the neural model and they just change their shape and size from one layer to another. If, in a quantization application, only a subset of these functions (model layers) is to be quantized, the quantization error will also flow through the non-quantized layers. Therefore, the model behavior will benefit more from calibrating every layer to reduce the quantization error than just calibrating the subset of layers that are being quantized. In this case, Equation 9 will be used to calibrate and quantize the layers that are being quantized, and Equation 8 will be used for non-quantized layers to just calibrate them.

4.3 Support for block-scaled data formats

Computing Equation 4 in hardware loops over the IFM dimension to calculate $o_{i,j} = \sum_{k=1}^{IFM} a_{i,k} * w_{j,k}$ (Figure 3, top middle). In a hardware realization of this operation, it is preferred to group the weights in the same direction for block-scaled number formats (Figure 3, top right). Using the notation in Equation 3, this loop is calculated as:

$$\sum_{k=1}^{IFM} a_{i,k} * w_{j,k} = \sum_{b=1}^{IFM/block_size} \left\{ s_b \times \sum_{k=1+(b-1)*block_size}^{b*block_size} a_{i,k} * v_{j,k} \right\} \quad (10)$$

This also means that each $v_{j,k}$ shares a block scale with a few other values in the k dimension and each block expands over multiple error matrices shown in Equation 5. Figure 3, right, displays the orthogonality of block direction and the direction of quantization correction.

And the block error matrix can be defined as $E_{block}^{(b)} = O_{block}^{(b)} - \widehat{O}_{block}^{(b)}$, and we use it to re-write our goal in Equation 6:

$$\tilde{O} + \sum_{b=1}^{IFM/block_size} \sum_{k=1+(b-1)*block_size}^{b*block_size} \widehat{A}_k (W_k^T - \widehat{W}_k^T) = 0 \quad (11)$$

Therefore, the update matrix for the block is:

$$U_{block}^{(b)} = \frac{\tilde{O}}{IFM/block_size} + E_{block}^{(b)} + U_{block}^{(b-1)} \quad (12)$$

All the values inside the block will be scaled with a shared scale. When processing step k , quantizing W_k may effect the scale calculation and could change the previously quantized values in the same block. At each step $(1 + (b - 1) * block_size \leq k \leq b * block_size)$, the block error $E_{block}^{(b)}$ should

be re-calculated. This means $U_{block}^{(b)}$ is updated at each iteration inside its block, b . In this case, at each iteration, l , inside the block, the following calculation is required:

$$l_update = \frac{\tilde{O}}{IFM/block_size} + \sum_{k=1+(b-1)*block_size, k \neq l}^{b*block_size} \hat{A}_k(W_k^T - \widehat{W}_k^T) + U_{block}^{(b-1)} \quad (13)$$

Note that the above sum skips over $k = l$. This is the total update term for the block minus step l . By evenly distributing this error among $block_size$ steps, at iteration l the update term is:

$$\widehat{W}_l^T = W_l^T + \frac{\hat{A}_l^T}{\|\hat{A}_l\|_2^2} \frac{l_update}{block_size} \quad (14)$$

Note that for $block_size = 1$, Equations 8 and 14 describe the same functions.

4.4 The Issue with the Large M

Similar to [19, 20], we also use multiple sample inputs for calibration. As explained in [19], the number of input samples linearly increases the size of M as it is equal to $input_size * number_of_samples$. This results in large memory requirement to store the error and update matrices. Equation 13’s three matrices, \tilde{O} , $U_{block}^{(b-1)}$, and $\hat{A}_k(W_k^T - \widehat{W}_k^T)$ are $M \times OFM$. To process each block, we can store the sum of the first two matrices as one entity and calculate the sum as following to minimize memory:

$$\sum_{k=1+(b-1)*block_size, k \neq l}^{b*block_size} \frac{\hat{A}_l^T \hat{A}_k}{\|\hat{A}_l\|_2^2} (W_k^T - \widehat{W}_k^T) \quad (15)$$

The term $\frac{\hat{A}_l^T \hat{A}_k}{\|\hat{A}_l\|_2^2}$ is a scalar and the above sum requires $1 \times OFM$ to store its results instead of $M \times OFM$. Additionally, one can pre-calculate all the $\frac{\hat{A}_l}{\|\hat{A}_l\|_2^2} (\tilde{O}/(IFM/block_size) + U_{block}^{(b-1)})$ and store a $block_size \times OFM$ matrix on chip instead of an $M \times OFM$ one. For example, if we use 256 samples for calibrating a fully connected layer in OPT [45] with input size 2048 and OFM size 8192, storing all three matrices in Equation 13 requires 3×2^{34} Bytes, while with pre-calculating and using Equation 15 for $block_size = 32$, we only need 2^{20} Bytes.

5 TensorCast

TensorCast is an open-source casting/quantization library based on PyTorch 2.2+. Its scope is defining number formats and converting tensors between them. It supports a variety of data formats, including the OCP MX datatypes described in [43] as well as additional data formats as needed to support research in the area of low precision for machine learning. TensorCast provides the needed infrastructure for researchers to describe new data formats and experiment with them to quantize neural models. The source code is available at github.com/ROCm/tensorcast.

6 Results

The ED algorithm simply selects the shared scale based on the largest-in-magnitude value in the block. Although improvements in better selecting the shared scale are part of our future work, our result section demonstrates that even with this initial approach, the results generated with block-scaled data formats are competitive with the tensor-scaled and row-scaled results achieved by other algorithms using a more compute costly tensor mean (GPFQ [19] with hyperparameters) or Hessian information (GPTQ [20]) to adjust their scale.

To our knowledge, ED is the first published PTQ algorithm that uses block-scaled data formats described in this text. We provide Table 1 to compare ED’s algorithm with row-scaled methods.

In this table, our results on image classification models show a clear advantage for ED over other methods. Some of the methods in Table 1 use a shared minimum in addition to the shared scale, which we do not use in the ED algorithm.

Model	Bits	ED	GPFQ[19]	MSE[46]	BRECQ[47]	AdaRound[39]	OMSE[48]
ResNet18	3	0.9679	0.9539	-	-	-	-
	4	0.9940	0.9826	0.9612	0.9940	0.9860	0.9819
ResNet50	3	0.9394	0.9431	-	-	-	-
	4	0.9910	0.9864	0.9697	0.9907	0.9889	0.9655

Table 1: Non block scaled data formats. Weights are quantized to int3 and int4 data formats. Results are normalized Top-1 accuracy (top-1 quantized divided by Top-1 baseline).

To compare our results with the SOTA PTQ methods used for LLMs, we compare them with the method explained in [20]. Table 2 shows our results with MX data formats [43] with per-block power-of-two shared scales against the Hessian-based algorithm using a per-row floating scale. The power-of-two scaling is cheaper in hardware implementation, and Table 2 shows competitive results with the MX data formats. In this table, the *ED+Calib* row includes the results of calibrating the last fully connected layer, as explained in subsection 4.2.

OPT	Bits	125M	350M	1.3B	2.7B	6.7B
Baseline	16	27.56	22.00	14.63	12.47	10.86
GPTQ	int4-fp	31.12	24.24	15.47	12.87	11.39
ED	mxint4	30.33	23.58	15.13	12.91	11.27
ED+Calib	mxint4	30.28	23.59	15.12	12.91	11.29
GPTQ	int3-fp	53.85	33.79	20.97	16.88	14.86
ED	mxint3	49.80	33.59	23.24	17.70	19.68
ED+Calib	mxint3	49.33	33.29	22.03	17.34	18.94

Table 2: Comparing float scaled per row [20] against power-of-two scaled MX data format [43] used in the ED algorithm on WikiText2.

As explained in section 4, we account for the change in activations after quantization ($A \neq \hat{A}$). With no modification in the algorithm, we apply quantization to activation and calibrate the weights. Table 3 displays our results on different models and datasets with activation and weight quantization with different four and six bit mini-float MX data formats.

Task	Family	Model	Dataset	Metric	FP32	MXFP6		MXFP4
						E2M3	E3M2	
Image Classification	Vision Transformer	DeiT-Tiny	ImageNet	Top-1	72.16	72.16	71.29	64.76
		DeiT-Small			80.54	80.50	80.25	76.80
	CNN	ResNet-18	ILSVRC12	Acc. ↑	70.79	70.66	70.15	67.40
		ResNet-19			77.40	77.15	76.48	69.99
		MobileNet v2			72.14	70.22	65.32	18.88
Speech Recognition	Transformer	Wav2Vec 2.0	LibriSpeech	WER ↓	18.90	19.09	19.6	24.39

Table 3: Both the activations and pre-trained weights from the baseline model are quantized to the column’s datatype.

7 Conclusions

This paper reviewed the block-scaled data formats and introduced the ED PTQ method. We explained the novel and hyperparameter-free structure of the ED algorithm for supporting these number formats and why calibrating all layers, including the ones kept in full precision improves the PTQ results. By having a shared scale, the block-scaled data formats introduce a dependency between the values inside the block. Therefore, selecting a good scale is a crucial step in the quantization process. Our results show that the low cost way of calculating the shared scale based on the largest absolute value in the block, these data formats can provide competitive results with a proper PTQ method. As for our future work, we plan to find ways to improve the shared scale calculation for PTQ of neural models.

8 Limitations

The ED algorithm introduced in this paper is the first PTQ method that uses the power of two block-scaled data formats. Shown results are comparable to float-scaled data formats. However, ED is not tested in cases where higher precision scales are needed (e.g., the presence of significant outliers in data). The sample size of the calibration data is fixed for each model class (e.g., OPT, ResNet) and is heuristically set to match the available GPU memory. The block-scaled data formats introduced in [43] are subject to change in future revisions. Although ED is not tested against future data formats, we believe our method should hold its performance.

References

- [1] Lei Deng, Guoqi Li, Song Han, Luping Shi, and Yuan Xie. Model compression and hardware acceleration for neural networks: A comprehensive survey. *Proceedings of the IEEE*, 108(4): 485–532, 2020. doi: 10.1109/JPROC.2020.2976475.
- [2] Vincent Vanhoucke, Andrew Senior, and Mark Z. Mao. Improving the speed of neural networks on cpus. In *Deep Learning and Unsupervised Feature Learning Workshop, NIPS 2011*, 2011.
- [3] Alfredo Canziani, Adam Paszke, and Eugenio Culurciello. An analysis of deep neural network models for practical applications, 2017. arXiv:1605.07678.
- [4] Kevin Siu, Dylan Malone Stuart, Mostafa Mahmoud, and Andreas Moshovos. Memory requirements for convolutional neural network hardware accelerators. In *2018 IEEE International Symposium on Workload Characterization (IISWC)*, pages 111–121, 2018. doi: 10.1109/IISWC.2018.8573527.
- [5] Shijin Zhang, Zidong Du, Lei Zhang, Huiying Lan, Shaoli Liu, Ling Li, Qi Guo, Tianshi Chen, and Yunji Chen. Cambricon-x: An accelerator for sparse neural networks. In *2016 49th Annual IEEE/ACM International Symposium on Microarchitecture (MICRO)*, pages 1–12, 2016. doi: 10.1109/MICRO.2016.7783723.
- [6] Kaiming He, Xiangyu Zhang, Shaoqing Ren, and Jian Sun. Deep residual learning for image recognition, 2015. arXiv:1512.03385.
- [7] Olaf Ronneberger, Philipp Fischer, and Thomas Brox. U-net: Convolutional networks for biomedical image segmentation, 2015. arXiv:1505.04597.
- [8] Olivia Weng, Gabriel Marcano, Vladimir Loncar, Alireza Khodamoradi, Abarajithan G, Nojan Sheybani, Andres Meza, Farinaz Koushanfar, Kristof Denolf, Javier Mauricio Duarte, and Ryan Kastner. Tailor: Altering skip connections for resource-efficient inference. *ACM Trans. Reconfigurable Technol. Syst.*, 17(1), jan 2024. ISSN 1936-7406. doi: 10.1145/3624990. URL <https://doi.org/10.1145/3624990>.
- [9] Ruofei Hu, Binren Tian, Shouyi Yin, and Shaojun Wei. Efficient hardware architecture of softmax layer in deep neural network. In *2018 IEEE 23rd International Conference on Digital Signal Processing (DSP)*, pages 1–5, 2018. doi: 10.1109/ICDSP.2018.8631588.
- [10] Zachariah Carmichael, Hamed F. Langroudi, Char Khazanov, Jeffrey Lillie, John L. Gustafson, and Dhireesha Kudithipudi. Performance-efficiency trade-off of low-precision numerical formats in deep neural networks. In *Proceedings of the Conference for Next Generation Arithmetic 2019, CoNGA’19*, New York, NY, USA, 2019. Association for Computing Machinery. ISBN 9781450371391. doi: 10.1145/3316279.3316282. URL <https://doi.org/10.1145/3316279.3316282>.
- [11] Nimit S. Sohoni, Christopher R. Aberger, Megan Leszczynski, Jian Zhang, and Christopher Ré. Low-memory neural network training: A technical report, 2022. arXiv:1904.10631.
- [12] Yunhui Guo. A survey on methods and theories of quantized neural networks, 2018. arXiv:1808.04752.

- [13] Amir Gholami, Sehoon Kim, Zhen Dong, Zhewei Yao, Michael W. Mahoney, and Kurt Keutzer. A survey of quantization methods for efficient neural network inference, 2021. arXiv:2103.13630.
- [14] Yanjing Li, Sheng Xu, Mingbao Lin, Xianbin Cao, Chuanjian Liu, Xiao Sun, and Baochang Zhang. Bi-vit: Pushing the limit of vision transformer quantization, 2023. arXiv:2305.12354.
- [15] Markus Nagel, Marios Fournarakis, Rana Ali Amjad, Yelysei Bondarenko, Mart van Baalen, and Tijmen Blankevoort. A white paper on neural network quantization, 2021. arXiv:2106.08295.
- [16] Andrey Kuzmin, Mart Van Baalen, Yuwei Ren, Markus Nagel, Jorn Peters, and Tijmen Blankevoort. Fp8 quantization: The power of the exponent, 2024. arXiv:2208.09225.
- [17] Peisong Wang, Qinghao Hu, Yifan Zhang, Chunjie Zhang, Yang Liu, and Jian Cheng. Two-step quantization for low-bit neural networks. In *2018 IEEE/CVF Conference on Computer Vision and Pattern Recognition*, pages 4376–4384, 2018. doi: 10.1109/CVPR.2018.00460.
- [18] Ron Banner, Itay Hubara, Elad Hoffer, and Daniel Soudry. Scalable methods for 8-bit training of neural networks. In S. Bengio, H. Wallach, H. Larochelle, K. Grauman, N. Cesa-Bianchi, and R. Garnett, editors, *Advances in Neural Information Processing Systems*, volume 31. Curran Associates, Inc., 2018. URL https://proceedings.neurips.cc/paper_files/paper/2018/file/e82c4b19b8151ddc25d4d93baf7b908f-Paper.pdf.
- [19] Jinjie Zhang, Yixuan Zhou, and Rayan Saab. Post-training quantization for neural networks with provable guarantees, 2023. arXiv:2201.11113.
- [20] Elias Frantar, Saleh Ashkboos, Torsten Hoefler, and Dan Alistarh. Gptq: Accurate post-training quantization for generative pre-trained transformers, 2023. arXiv:2210.17323.
- [21] Guangxuan Xiao, Ji Lin, Mickael Seznec, Hao Wu, Julien Demouth, and Song Han. Smoothquant: Accurate and efficient post-training quantization for large language models, 2024. arXiv:2211.10438.
- [22] Eunhyeok Park, Dongyoung Kim, and Sungjoo Yoo. Energy-efficient neural network accelerator based on outlier-aware low-precision computation. In *2018 ACM/IEEE 45th Annual International Symposium on Computer Architecture (ISCA)*, pages 688–698, 2018. doi: 10.1109/ISCA.2018.00063.
- [23] William Kahan. A survey of error analysis. In *IFIP Congress*, 1971. URL <https://api.semanticscholar.org/CorpusID:7319965>.
- [24] Holger Scherl. *FPGA-Based Hardware*, pages 89–96. Vieweg+Teubner, Wiesbaden, 2011. ISBN 978-3-8348-8259-2. doi: 10.1007/978-3-8348-8259-2_7. URL https://doi.org/10.1007/978-3-8348-8259-2_7.
- [25] Bitarouhani, Ritchie Zhao, Ankit More, Mathew Hall, Alireza Khodamoradi, Summer Deng, Dhruv Choudhary, Marius Cornea, Eric Dellinger, Kristof Denolf, Stosic Dusan, Venmugil Elango, Maximilian Golub, Alexander Heinecke, Phil James-Roxby, Dharmesh Jani, Gaurav Kolhe, Martin Langhammer, Ada Li, Levi Melnick, Maral Mesmakhosroshahi, Andres Rodriguez, Michael Schulte, Rasoul Shafipour, Lei Shao, Michael Siu, Pradeep Dubey, Paulius Micikevicius, Maxim Naumov, Colin Verrilli, Ralph Wittig, Doug Burger, and Eric Chung. Microscaling data formats for deep learning, 2023. arXiv:2310.10537.
- [26] Bitarouhani, Ritchie Zhao, Venmugil Elango, Rasoul Shafipour, Mathew Hall, Maral Mesmakhosroshahi, Ankit More, Levi Melnick, Maximilian Golub, Girish Varatkar, Lei Shao, Gaurav Kolhe, Dimitry Melts, Jasmine Klar, Renee L’Heureux, Matt Perry, Doug Burger, Eric Chung, Zhaoxia Deng, Sam Naghshineh, Jongsoo Park, and Maxim Naumov. With shared microexponents, a little shifting goes a long way, 2023. arXiv:2302.08007.
- [27] Bitarouhani, Daniel Lo, Ritchie Zhao, Ming Liu, Jeremy Fowers, Kalin Ovtcharov, Anna Vinogradsky, Sarah Massengill, Lita Yang, Ray Bittner, Alessandro Forin, Haishan Zhu, Taesik Na, Prerak Patel, Shuai Che, Lok Chand Koppaka, XIA SONG, Subhojit Som, Kaustav Das, Saurabh T, Steve Reinhardt, Sitaram Lanka, Eric Chung, and Doug Burger.

- Pushing the limits of narrow precision inferencing at cloud scale with microsoft floating point. In H. Larochelle, M. Ranzato, R. Hadsell, M.F. Balcan, and H. Lin, editors, *Advances in Neural Information Processing Systems*, volume 33, pages 10271–10281. Curran Associates, Inc., 2020. URL https://proceedings.neurips.cc/paper_files/paper/2020/file/747e32ab0fea7fbd2ad9ec03daa3f840-Paper.pdf.
- [28] Eunhyeok Park, Sungjoo Yoo, and Peter Vajda. Value-aware quantization for training and inference of neural networks, 2018. arXiv:1804.07802.
- [29] Zhongnan Qu, Zimu Zhou, Yun Cheng, and Lothar Thiele. Adaptive loss-aware quantization for multi-bit networks, 2020. arXiv:1912.08883.
- [30] Mingzhu Shen, Feng Liang, Ruihao Gong, Yuhang Li, Chuming Li, Chen Lin, Fengwei Yu, Junjie Yan, and Wanli Ouyang. Once quantization-aware training: High performance extremely low-bit architecture search. In *Proceedings of the IEEE/CVF International Conference on Computer Vision (ICCV)*, pages 5340–5349, October 2021.
- [31] Markus Nagel, Marios Fournarakis, Yelysei Bondarenko, and Tijmen Blankevoort. Overcoming oscillations in quantization-aware training. In Kamalika Chaudhuri, Stefanie Jegelka, Le Song, Csaba Szepesvari, Gang Niu, and Sivan Sabato, editors, *Proceedings of the 39th International Conference on Machine Learning*, volume 162 of *Proceedings of Machine Learning Research*, pages 16318–16330. PMLR, 17–23 Jul 2022.
- [32] Sheng Shen, Zhen Dong, Jiayu Ye, Linjian Ma, Zhewei Yao, Amir Gholami, Michael W. Mahoney, and Kurt Keutzer. Q-bert: Hessian based ultra low precision quantization of bert, 2019. arXiv:1909.05840.
- [33] Pedro J. Freire, Antonio Napoli, Bernhard Spinnler, Michael Anderson, Diego Argüello Ron, Wolfgang Schairer, Thomas Bex, Nelson Costa, Sergei K. Turitsyn, and Jaroslaw E. Prilepsky. Reducing computational complexity of neural networks in optical channel equalization: From concepts to implementation. *Journal of Lightwave Technology*, 41(14):4557–4581, 2023. doi: 10.1109/JLT.2023.3234327.
- [34] Jordan Hoffmann, Sebastian Borgeaud, Arthur Mensch, Elena Buchatskaya, Trevor Cai, Eliza Rutherford, Diego de Las Casas, Lisa Anne Hendricks, Johannes Welbl, Aidan Clark, Thomas Hennigan, Eric Noland, Katherine Millican, George van den Driessche, Bogdan Damoc, Aurelia Guy, Simon Osindero, Karén Simonyan, Erich Elsen, Oriol Vinyals, Jack Rae, and Laurent Sifre. An empirical analysis of compute-optimal large language model training. In S. Koyejo, S. Mohamed, A. Agarwal, D. Belgrave, K. Cho, and A. Oh, editors, *Advances in Neural Information Processing Systems*, volume 35, pages 30016–30030. Curran Associates, Inc., 2022. URL https://proceedings.neurips.cc/paper_files/paper/2022/file/c1e2faff6f588870935f114ebe04a3e5-Paper-Conference.pdf.
- [35] Jordan Hoffmann, Sebastian Borgeaud, Arthur Mensch, Elena Buchatskaya, Trevor Cai, Eliza Rutherford, Diego de Las Casas, Lisa Anne Hendricks, Johannes Welbl, Aidan Clark, Tom Hennigan, Eric Noland, Katie Millican, George van den Driessche, Bogdan Damoc, Aurelia Guy, Simon Osindero, Karen Simonyan, Erich Elsen, Jack W. Rae, Oriol Vinyals, and Laurent Sifre. Training compute-optimal large language models, 2022. arXiv:2203.15556.
- [36] Micah Musser. A cost analysis of generative language models and inference operations, 2023.
- [37] Yury Nahshan, Brian Chmiel, Chaim Baskin, Evgenii Zheltonozhskii, Ron Banner, Alex M. Bronstein, and Avi Mendelson. Loss aware post-training quantization, 2020. arXiv:1911.07190.
- [38] Benoit Jacob, Skirmantas Kligys, Bo Chen, Menglong Zhu, Matthew Tang, Andrew Howard, Hartwig Adam, and Dmitry Kalenichenko. Quantization and training of neural networks for efficient integer-arithmetic-only inference, 2017. arXiv:1712.05877.
- [39] Markus Nagel, Rana Ali Amjad, Mart van Baalen, Christos Louizos, and Tijmen Blankevoort. Up or down? adaptive rounding for post-training quantization, 2020. arXiv:2004.10568.
- [40] Elias Frantar, Sidak Pal Singh, and Dan Alistarh. Optimal brain compression: A framework for accurate post-training quantization and pruning, 2023. arXiv:2208.11580.

- [41] Yann LeCun, John Denker, and Sara Solla. Optimal brain damage. In D. Touretzky, editor, *Advances in Neural Information Processing Systems*, volume 2. Morgan-Kaufmann, 1989. URL https://proceedings.neurips.cc/paper_files/paper/1989/file/6c9882bbac1c7093bd25041881277658-Paper.pdf.
- [42] B. Hassibi, D.G. Stork, and G.J. Wolff. Optimal brain surgeon and general network pruning. In *IEEE International Conference on Neural Networks*, pages 293–299 vol.1, 1993. doi: 10.1109/ICNN.1993.298572.
- [43] OCP. Amd, arm, intel, meta, microsoft, nvidia, and qualcomm standardize next-generation narrow precision data formats for ai. opencompute.org, 2023. Accessed: May 06 2024.
- [44] AMD. Amd instinct™ mi300x accelerators. amd.com, 2023. Accessed: 2023-05-14.
- [45] Susan Zhang, Stephen Roller, Naman Goyal, Mikel Artetxe, Moya Chen, Shuohui Chen, Christopher Dewan, Mona Diab, Xian Li, Xi Victoria Lin, Todor Mihaylov, Myle Ott, Sam Shleifer, Kurt Shuster, Daniel Simig, Punit Singh Koura, Anjali Sridhar, Tianlu Wang, and Luke Zettlemoyer. Opt: Open pre-trained transformer language models, 2022. arXiv:2205.01068.
- [46] Ron Banner, Yury Nahshan, Elad Hoffer, and Daniel Soudry. Post-training 4-bit quantization of convolution networks for rapid-deployment, 2019. arXiv:1810.05723.
- [47] Yuhang Li, Ruihao Gong, Xu Tan, Yang Yang, Peng Hu, Qi Zhang, Fengwei Yu, Wei Wang, and Shi Gu. Brecq: Pushing the limit of post-training quantization by block reconstruction, 2021. arXiv:2102.05426.
- [48] Yoni Choukroun, Eli Kravchik, Fan Yang, and Pavel Kisilev. Low-bit quantization of neural networks for efficient inference, 2019. arXiv:1902.06822.